Clim Dyn (2006) 27:613–625
DOI 10.1007/s00382-006-0159-z

Ice-free glacial northern Asia due to dust deposition on snow

Gerhard Krinner · Olivier Boucher · Yves Balkanski

Received: 28 September 2005 / Accepted: 12 May 2006 / Published online: 13 June 2006

Abstract During the Last Glacial Maximum (LGM, 21 kyr BP), no large ice sheets were present in northern Asia, while northern Europe and North America (except Alaska) were heavily glaciated. We use a general circulation model with high regional resolution and a new parameterization of snow albedo to show that the ice-free conditions in northern Asia during the LGM are favoured by strong glacial dust deposition on the seasonal snow cover. Our climate model simulations indicate that mineral dust deposition on the snow surface leads to low snow albedo during the melt season. This, in turn, caused enhanced snow melt and therefore favoured snow-free peak summer conditions over almost the entire Asian continent during the LGM, whereas perennial snow cover is simulated over a large part of eastern Siberia when glacial dust deposition is not taken into account.

G. Krinner (✉)
LGGE, CNRS-UJF Grenoble, BP 96,
38402 Saint Martin d'Hères, France
e-mail: krinner@ujf-grenoble.fr

O. Boucher
LOA, CNRS-Université des Sciences et Technologies de Lille, 59655 Villeneuve d'Ascq, France

Present Address:
O. Boucher
Hadley Centre for Climate Prediction and Research, Met Office, FitzRoy Road, Exeter EX1 3PB, UK

Y. Balkanski
LSCE, CEA/CNRS Saclay, 91191 Gif sur Yvette Cedex, France

1 Introduction

Northern Asia and Alaska were essentially ice-free during the Last Glacial Maximum (LGM)(Clark and Lix 2002; Svendsen et al. 2004) in spite of very cold climatic conditions (Hubberten et al. 2004). At the same time, northern Europe and northern North America (except Alaska) were heavily glaciated (Clark and Lix 2002; Svendsen et al. 2004). The reason for this intriguingly contrasting ice extent is unclear. Under LGM conditions, climate models often tend to produce perennial snow cover at least in some parts of Asia and/or Alaska that were ice-free at that time. For example, 10 out of 15 models participating in the Paleoclimate Modeling Intercomparison Project (PMIP: Joussaume and Taylor 1995) do so, implying that the effect of glacial cooling overcompensates for the general drying. For several of the remaining five models, the fact that they do not produce perennial snow cover in these regions appears to be linked to significant warm biases in their simulation of present-day polar climate. Several climate processes will in general determine together the various terms of the surface mass balance of an ice sheet. Summer melt, for example, is determined by a variety of climatic parameters (air temperature, insolation, surface wind speed, surface albedo, etc.), which in turn are consequences of diverse local and remote factors such as atmospheric circulation patterns, oceanic moisture sources, ice sheet configuration, moisture and energy sources near the ice sheet margin (e.g. proglacial lakes), and deposition of impurities such as dust. Here, we will concentrate on the effect of the deposition of mineral dust on snow albedo and thus on snow melt during the LGM (21 kyr BP).

Glacial deposition rates of mineral dust (Mahowald et al. 1999) were very high on the global scale, and particularly so over Asia because of the short distance to strong mineral dust sources such as the Gobi desert. Figure 1 illustrates this coincidence of ice-free conditions and high mineral dust (hereafter ''dust'') accumulation rates over Asia during the LGM (the figure also indicates some areas which will be referred to later in the text). Several studies of the impact of atmospheric dust aerosols on the regional radiative balance have been carried out in the past. Liao and Seinfeld (1998) clearly show that atmospheric dust exerts a positive radiative forcing over bright surfaces. Overpeck et al. (1996) showed that the high dust loading in the atmosphere can induce significant warming over snow-covered regions, thereby contradicting earlier studies (e.g. Harvey 1988). However, model experiments suggest that in tropical regions, where surface albedo is low, the radiative impact of increased glacial dust loading in the atmosphere was of the same sign and magnitude of the radiative forcing of the low glacial CO_2 levels (e.g. Harrison et al. 2001). Atmospheric dust loading also has indirect radiative effects, because dust particles can act as cloud condensation nuclei. Cloud reflectivity and lifetime are therefore influenced by aerosols (Haywood and Boucher 2000; Takemura et al. 2005), but these indirect radiative impacts are difficult to assess.

Once deposited on the surface, dust can continue to influence the Earth's radiative balance. Dust deposition decreases the albedo of a snow surface. Peltier and Marshall (1995) have shown the importance of glacial dust deposition in facilitating deglaciation after the LGM. Similarly, in a study of glacial inception around 120 ka BP, Calov et al. (2005) have shown that LGM-type dust deposition can have major impacts on the ice sheet mass balance, and thus on the climate dynamics, at that period. On ice-free regions, the effect of dust deposition can induce increased summer melt of a seasonal snow cover, and thus hinder the establishment of an ice sheet. In spite of the importance of these potential consequences, however, this effect has not been quantified yet for ice-free regions subject to long seasonal snow cover. This study addresses this question by carrying out a general circulation model (GCM) sensitivity study on the impact of dust deposition on snow surfaces. We focus on the Asian continent, where, as stated before, elevated dust deposition rates tend to coincide with the absence of significant ice cover at the LGM, suggesting that, among other factors such as atmospheric moisture and energy advection, dust deposition was one of the processes that determined the glacial ice sheet extent.

2 Methods

We used the LMDZ4 (Laboratoire de Météorologie Dynamique, CNRS Paris) atmospheric GCM (Hourdin et al. 2006) to quantify the impact of mineral dust (hereafter ''dust'') deposition on the mass balance of seasonal snow covers under LGM climate conditions.

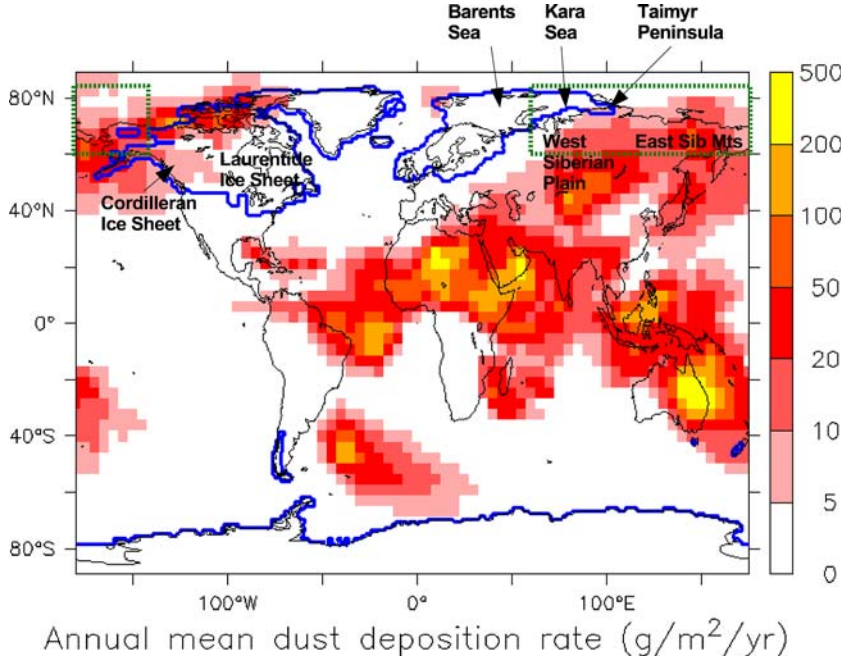

Fig. 1 Annual mean dust deposition rate at the LGM (*shading*; Mahowald et al. 1999) and LGM ice sheet extent (*blue lines*; Peltier 2004). The figure also indicates the location of regions referred to in the text. The *green rectangles* indicate the ''region of interest'' as defined in the text

For this work, the old snow albedo and snow cover fraction parameterization by Chalita and Le Treut (1994) was replaced by a new formulation in which snow albedo and fraction is calculated separately for forests, grasslands/deserts, and ice sheets. Following Douville et al. (1995) and Roesch et al. (2001), the parameterization of snow cover fraction over grasslands and deserts takes into account subgrid-scale orographic variability, which reduces snow cover fraction over mountainous terrain. In forests, interception of snow by leaves (dependent on leaf area index) and branches, unloading of snow as a function of wind and temperature, and the snow cover fraction on trees is represented following Roesch et al. (2001). Snow cover fraction on forest ground is calculated using the snow cover fraction formulation of Chalita and Le Treut (1994) with a roughness length of 2 cm. Snow albedo for forest soil is modified compared to other surface types by taking into account the accumulation of plant debris with age (Brun et al. 1989).

For calculating the dust content of the snow, the snow pack is represented by using a two-layer model, with a surface layer of maximum thickness $h_{s,max}$ = 8 mm (water equivalent; sensitivity tests with a maximum surface layer thickness of $h_{s,max}$ = 2 cm yielded similar results) and a bottom layer containing the remaining snow mass. This type of vertical discretization was chosen because far from the source regions, dust particles in the northern Hemisphere generally have a mean size of a few microns, both during glacial and interglacial periods (Guelle et al. 2000; Steffensen 1997). Dust particles of this size are not flushed through the snow layer during snow melt (Aoki et al. 2003; Jacobson 2004). Meltwater is generated preferentially near the surface, where the energy balance during the melt season is positive, while the dust particles tend to stay in place. This leads to 1-cm-thick dirty snow layer at the surface, widely used to visually identify summer horizons in alpine firn cores and represented here as the surface layer. If the total snow height h is less than $h_{s,max}$, the bottom layer thickness h_b is set to 0 and the surface layer thickness $h_s = h$; otherwise, $h_s = h_{s,max}$ and $h_b = h - h_s$.

The mineral dust content D of the snow (kg/kg) is a prognostic variable in each layer. During snow accumulation, the dust content in the surface layer is recalculated assuming that fresh snow is pure, and the total dust mass in the snow is conserved by adjusting the dust content in the bottom layer correspondingly. The surface layer accumulates dust from atmospheric fallout as well as from the lower layer during snow melt or sublimation, but loses dust through flushing. Fallout is supposed to occur as dry deposition at a constant annual mean rate C (kg/m^2/day), increasing the dust content in the surface layer: $dD_s/dt = C/(\rho h_s)$, where ρ is the prescribed constant snow density (330 kg/m^3). The constant deposition rate from the atmosphere is a conservative assumption, because at present, dust deposition in Asia is usually strongest during spring (Qian et al. 2002), increasing the impact of dust on snow melt. During melt or sublimation, snow mass is supposed to be lost from the surface layer. The dust mass corresponding to the lost snow height remains in the surface layer, which is then extended downwards to attain again the maximum thickness $h_{s,max}$ if possible (i.e., if enough snow remains in the bottom layer). For the dust content in the surface layer, this yields $D_s = (D_s' h_s' + \min(L, h_b') D_b')/h_s$, where L denotes the snow height lost during the time step and the primes indicate that the values of the variables at the preceding time step are taken. When the snow height falls below 1 mm water equivalent, D_s is not recalculated in order to prevent numerical divergence. The dust content in the bottom layer is not modified during this process. Although, as stated before, small dust particles tend to remain in place during snow melt, we conservatively assume flushing of dust particles in both snow layers during melting conditions with a time constant of τ = 15 days, that is: $dD/dt = -D/\tau$.

Snow albedo is estimated using the theory of Wiscombe and Warren (1980) and Warren and Wiscombe (1980), who validated their model for cases of pure snow and for snow containing aerosols; our model yields results equivalent to those reported by Warren and Wiscombe (1980) for given aerosol concentrations. The snow albedo of the bottom layer is computed first for diffuse radiation as a function of the underlying surface albedo, snow grain size, and dust content. This albedo of the bottom layer is then used as the underlying albedo when computing the albedos of the surface layer (for direct and diffuse radiation) which also depend on the dust content and snow grain size. Snow grain size evolves prognostically as a function of snow age and temperature (Marshall and Oglesby 1994), but unlike the dust content, it takes the same value in both snow layers. The snow albedo is averaged spectrally in the visible and near-infrared spectrum. Refractive indices for ice are taken from the GEISA database (Jacquinet-Husson et al. 1999). Mineral dust is assumed to follow a log-normal size distribution with a median mass diameter of 2.0 μm (Guelle et al. 2000), and its refractive index is computed according to its haematite content (Claquin et al. 1999).

Simulated present and glacial dust deposition rates (Mahowald et al. 1999) were prescribed in the climate model. The grid-stretching capability of LMDZ4 al-

lows high horizontal resolution (100 km) over northern Siberia at low computational cost (Krinner et al. 2004). The present-day simulations used the monthly mean 1979–1993 sea surface boundary conditions from the atmospheric model intercomparison project (AMIP: Gates 1992). The LGM simulations were constrained by appropriate ice sheet reconstructions (Peltier 2004), sea surface conditions (CLIMAP project members 1984), greenhouse gas concentrations (Petit et al. 1999), vegetation reconstructions (Crowley 1995), and insolation (Berger 1978) as boundary conditions. As the optical properties of eolian dust depend critically on its haematite content (Claquin et al. 2003), four simulations were carried out for each period: one with no dust deposition (called "ND/Xk", where "X" is 0 or 21, depending on the period considered), and three with varying haematite content (0.5%: "D0.5/Xk", 1.5%: "D1.5/Xk", and 3.5%: "D3.5/Xk"), representing the minimum, average, and maximum haematite contents in a $4° \times 5°$ global database of arid soil surface mineralogy (Claquin et al. 1999). The results of the dust simulations with 0.5, 1.5, and 3.5% haematite content are very similar, particularly as far as minimum seasonal snow cover extent is concerned. Moreover, 1.5% appears to be the most realistic mean haematite content of the dust deposited in northern Asia, because this is the typical haematite fraction in the Central Asian dust source regions (Claquin et al. 1999). For these reasons, only the D1.5 and ND simulations will generally be discussed in the following. The present-day simulations were run over 9 years, of which the first 2 years were discarded as spinup. Because the annual minimum snow cover extent attained its equilibrium only after 7 years in simulation ND/21k, it was run over 32 years, the first 20 years being discarded as spinup. To ensure consistency between ND/21k and D1.5/21k, D1.5/21k was run following the same protocol (32 years of simulation, with 20 years of spinup), although no noticeable trend was seen in the annual maximum and minimum snow cover extent in D1.5/21k between year 3 and 32.

3 Results

3.1 Present-day climate

Present-day simulated annual mean surface air temperatures in this region compare favourably with observations (Legates and Willmott 1990), with a negligible mean bias (0.0°C) and a mean absolute error of 1.4°C (Fig. 2).

Compared to observations for the period 1979–1993 (Beck et al. 2005), the simulated present-day snow cover duration in Alaska and northern Asia (60°E to 220°E; > 60°N, hereafter referred to as the "region of interest") is overestimated over mountainous regions, such as the Brooks Range in northern Alaska or the east Siberian mountain ranges, where annual mean precipitation is locally overestimated by a factor of up to three. An increase of simulated orographic resolution is often obtained when model resolution is refined. In our case however, the overestimate of precipitation over the east Siberian mountain ranges does not seem to be related to the relatively high model resolution. Tests with regular grid simulations at about 300 km resolution, using the same model, yielded the same bias (not shown). In flat regions, such as the West Siberian

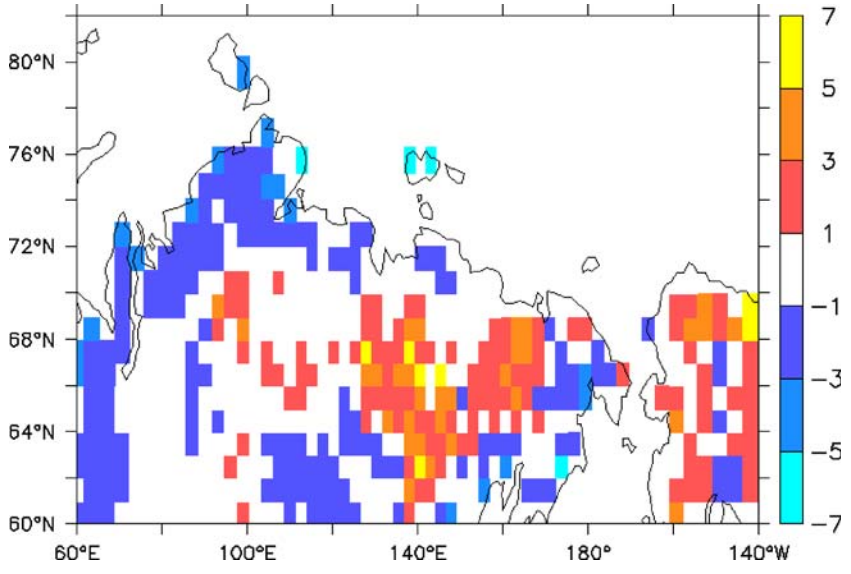

Fig. 2 Annual mean surface air temperature bias for simulation D1.5/0k (°C)

Plain, the simulated precipitation agrees well with the observations. On average, precipitation over the region of interest is overestimated by about 50%. Given the fairly low observed precipitation amounts (less than 300 mm/year in most of the region of interest), this overestimate is weak in absolute terms.

The precipitation bias is strongest in summer, but it still leads to an overestimate of the present-day snow cover duration in the region of interest. Compared to satellite observations (Armstrong and Brodzik 2002), snow cover duration is overestimated by about 2 weeks on average in all present-day simulations (Fig. 3). The bias attains almost two months over the east Siberian mountain ranges. Due to low present-day dust deposition rates, the climatic impact of dust deposition on snow in the various present-day simulations, with their varying prescribed haematite content in dust, is negligible everywhere. It is therefore not shown.

3.2 LGM climate and impact of dust deposition on snow

Similar to various estimates (Hubberten et al. 2004; Tarasov et al. 1999) and previous climate simulations (Siegert and Marsiat 2001), the simulated glacial climate is much dryer than the present climate over Western Siberia, with precipitation being reduced by about 50% (Fig. 4). Further east, the precipitation reduction is weaker. Locally, simulated LGM precipitation rates even exceed present-day values there.

Estimates derived from pollen and plant macrofossils (Tarasov et al. 1999) indicate a mean cooling (i.e. surface air temperature difference between the LGM and present) of the coldest month of about 9°C in the region of interest. The cooling is about 4°C too strong in the simulation without dust; in D1.5/21k, the cooling is at the lower end of the reconstruction taking into account reconstruction uncertainties. Because of weak solar radiation and low dust concentration on the surface snow during winter, the difference between the simulations with and without dust is not very strong during that season; the signal is linked to a slightly weaker winter surface albedo in D1.5/21k, caused by a small dust-induced snow albedo decrease and by a similarly small reduction of snow cover fraction (due to partial shielding of the snow surface by roughness elements because of the much lower snow thickness than in ND/21k).

The situation is different in summer. In the areas which are continental both at present and at the LGM, the simulated cooling during the warmest month is typically about –6°C in D1.5/12k and between –17 and –7°C in D0/21k (Fig. 5). In regions where present-day ocean is replaced by land at the LGM (in the Bering Strait and along the north coasts of Siberia and Alaska), the warmest month at the LGM can be warmer than at present. This is due to a higher amplitude of the seasonal temperature cycle over land than over the sea, in particular in D1.5/21k, where these regions are snow-free in summer, as will be shown later. Compared to the estimates for Western Siberia by Tarasov et al. (1999), the simulated cooling of the warmest month is 2.0°C too strong in the D1.5 simulations, which is still within the uncertainty of the climate reconstructions. In the simulations without dust, the simulated cooling of the warmest month is 8°C too strong, clearly exceeding the uncertainty of the reconstructions. Further south, the model bias is weaker. However, the

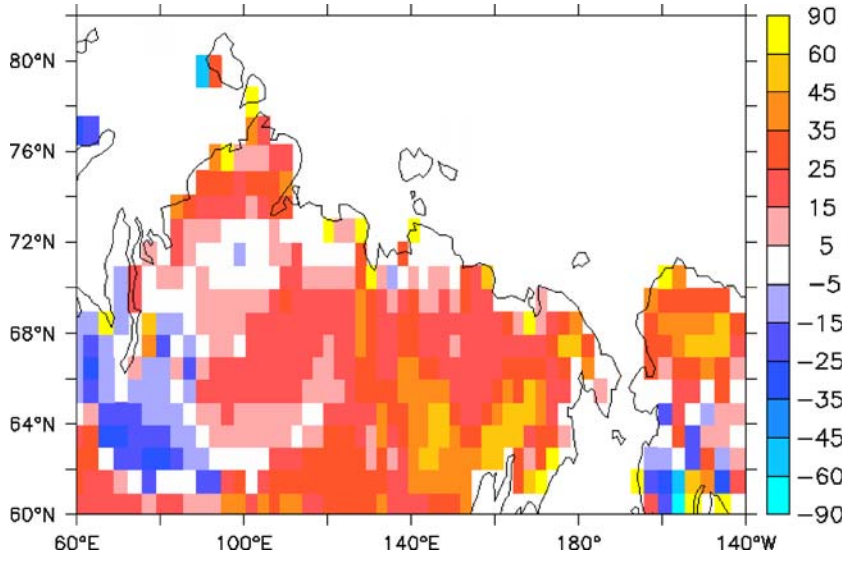

Fig. 3 Bias of the simulated snow cover duration (simulation D1.5/0k, in days) with respect to satellite data (Armstrong and Brodzik 2002)

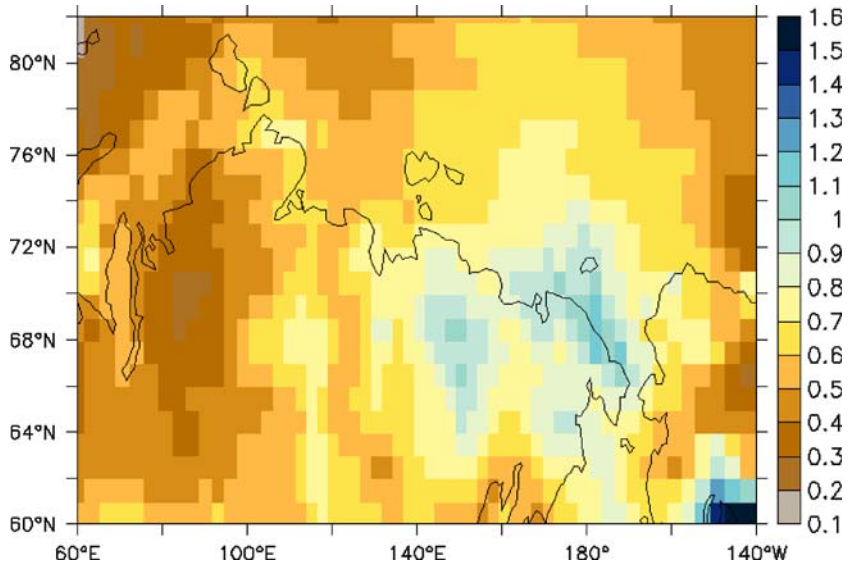

Fig. 4 Ratio between LGM annual mean precipitation (D1.5/21k) and present-day annual mean precipitation (D1.5/0k)

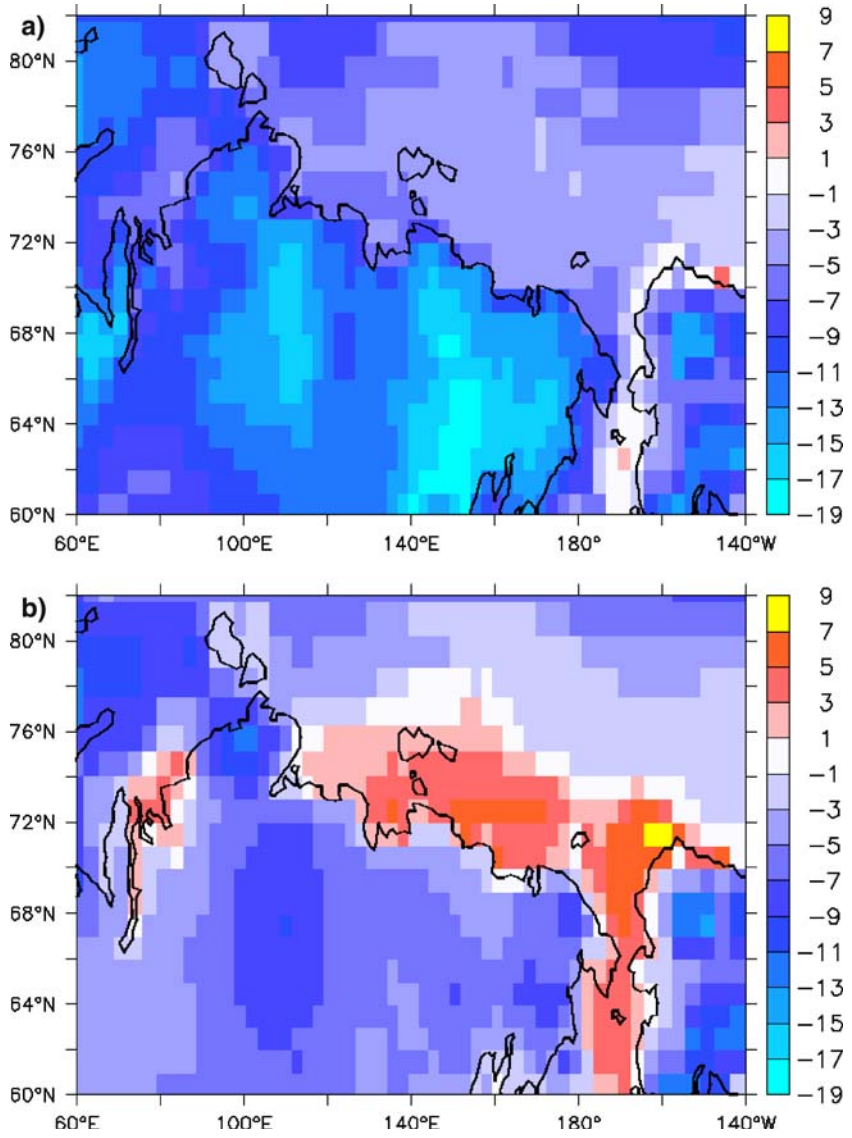

Fig. 5 Simulated LGM minus present surface air temperature difference of the warmest month. **a** D0/21k – D0/0k and **b** D1.5/21k – D1.5/0k

simulations without dust still overestimate the glacial summer cooling by 4°C if the region is extended south to 55°N. The strong overestimate of the summer cooling in the simulations without dust is linked to simulated permanent snow cover, as will be shown in the following.

Ice sheet inception occurs when snow cover becomes permanent, that is, when the number of snow-free days per year is zero. This is the diagnostic variable of interest here in terms of climate dynamics. Figure 6 displays this number of snow-free days (hereafter NSFD) in ND/21k and D1.5/21k, and the difference between D1.5/21k-ND/21k, that is, the change due to the dust deposition on the snow surface. The total area of simulated permanent snow cover (excluding ice sheets) in the North Asian/Alaskan region of interest is 3.4×10^6 km^2 in ND/21k, and almost seven times less (4.9×10^5 km^2) in D1.5/21k. Without mineral dust, the model simulates permanent glacial snow cover along the southwestern margin of the Barents Ice Sheet, along the whole northern coast of Asia, over the entire Russian Far East, and, interestingly, over Tibet. In D1.5/21k, permanent snow cover (excluding ice sheets) only occurs over Severnaya Zemlya, where localized ice caps existed at the LGM (Makeyev and Bolshiyanov 1986), and in the northern part of the Taimyr Peninsula, where at least partial glaciation during the LGM is thought possible (Svendsen et al. 2004). In ice-free regions where permanent snow cover is simulated in D0/21k, snow-free conditions generally prevail during more than a month, locally more than two months, in D1.5/21k.

The strong difference between D1.5/21k and ND/21k is due to dust deposition on snow and feedbacks within the model. Figure 7 displays a time series of monthly surface albedo, surface dust concentration and snow mass as simulated in D1.5/21k at 166°E and 63.5°N. This is one of the grid points that remain free of permanent snow cover in D1.5/21k, but not in ND/21k. The figure illustrates how the onset of snow melt in early summer leads to increased concentration of dust in the surface layer of the snow cover, which in turn induces higher melt rates. This positive feedback leads to snow-free peak summer conditions. As stated before, due to low present-day dust deposition rates, this feedback does not operate on large spatial scales today, neither in reality nor in our simulations.

4 Discussion

We do not pretend that dust deposition was the only factor determining the glacial ice sheet configuration. However, our simulations suggest that dust deposition on snow during the LGM in northern Asia lead to increased snow-melt in summer, thus impeding ice sheet inception in this region even during peak glacial times, possibly in conjunction with other factors such as weak precipitation rates.

In this paper, we focused on the D1.5 simulations, that is, we supposed a 1.5% haematite content in the dust, because this is the most probable value in northern Asia (Claquin et al. 1999). As stated before, the results for the 0.5% case are very similar in terms of extent of permanent snow cover in the region of interest. Indeed, both simulations (D1.5/21k and D0.5/21k) suggest that an area of 4.9×10^5 km^2 is covered by permanent snow, compared to 3.4×10^6 km^2 in D0/21k.

It would be interesting to examine the impact of dust deposition at other glacial periods. Varying widely in association with Dansgaard-Oeschger and Heinrich events (Mayewski et al. 1994), dust concentration in the GRIP ice core from Central Greenland exceeded 33% of peak glacial values repeatedly for millennia during the middle and late Weichselian glaciation after about 85 kyr BP (Fuhrer et al. 1999). Unfortunately, dust deposition maps for time slices other than the present and the LGM are not available. We therefore carried out additional LGM dust simulations with the dust deposition rate reduced by a factor three and a 1.5% haematite content. This simulation is designed to test the impact of lower dust deposition at earlier glacial stages. The results of this ''reduced deposition rate'' simulation are very similar to those of the ''full deposition rate'' simulation D1.5/21k, except that local glaciation occurs over parts of the East Siberian mountain ranges. In this region, traces of local glaciations before the LGM, when dust deposition rates were reduced, have indeed been found (Stauch et al. 2005). We conclude that the impact of dust deposition on snow was also important during glacial times with much weaker dust deposition than at the LGM.

Over Western Siberia, the strong precipitation reduction at the LGM certainly contributed to the ice-free conditions, as suggested previously (Hubberten et al. 2004; Siegert and Marsiat 2001). However, the dust deposition enhances the number of snow-free days over the whole region. More locally, the model even suggests dust-induced recession of permanent snow cover along the southeastern margin of the Scandinavian/Barents Ice Sheet (around 60°E/70°N). Recent field data and ice sheet reconstructions (Svendsen et al. 2004) indicate that the ice sheet extended significantly further to the East only during the Early Weichselian and retreated after 90 kyr BP.

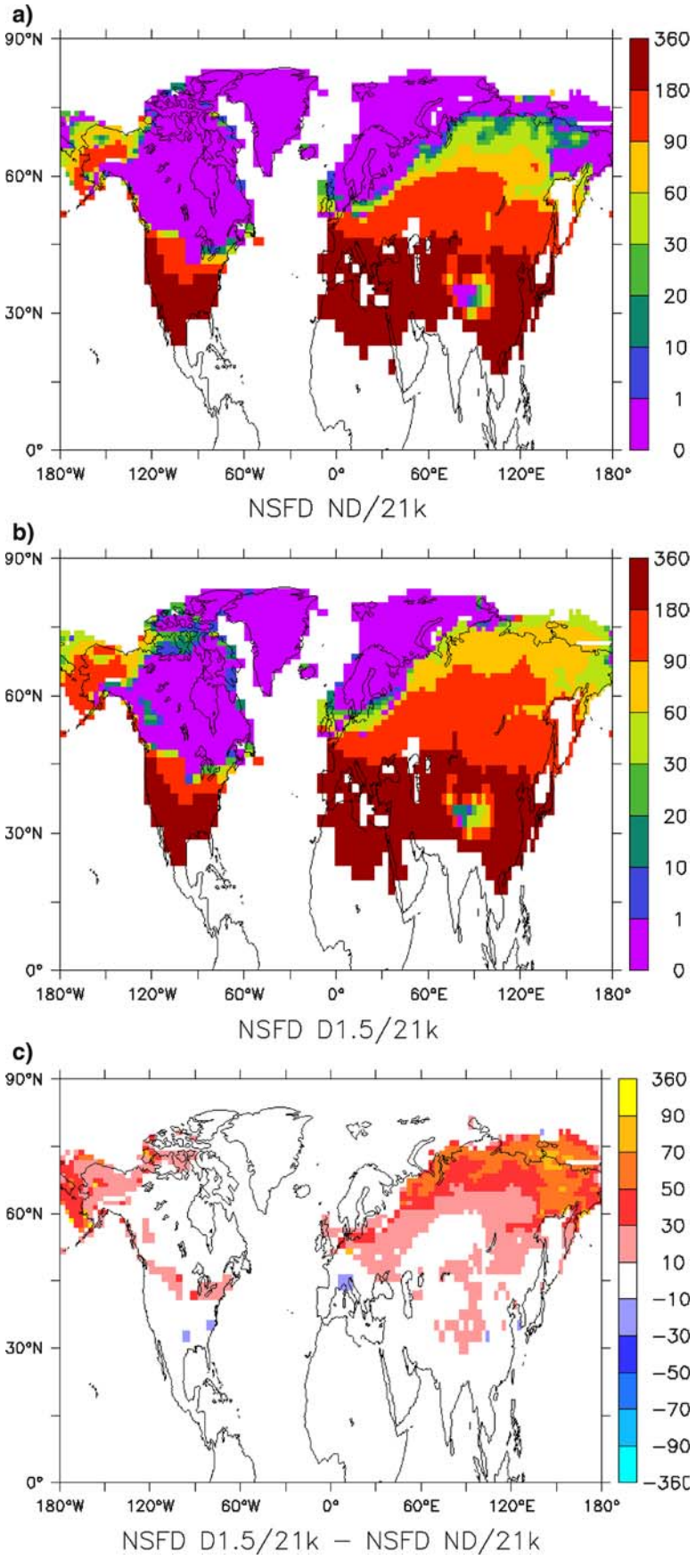

Fig. 6 Number of snow-free days per year (*NSFD*) over the continents. **a** *NSFD* simulated in ND/21k, **b** *NSFD* simulated in D1.5/21k and **c** *NSFD* difference: D1.5/21k – ND/21k. Widespread glacial inception over Northern Siberia occurs in ND/21k. *White zones* in (**a**) and (**b**) indicate oceanic grid points or continental grid points without any snow at all during the whole year

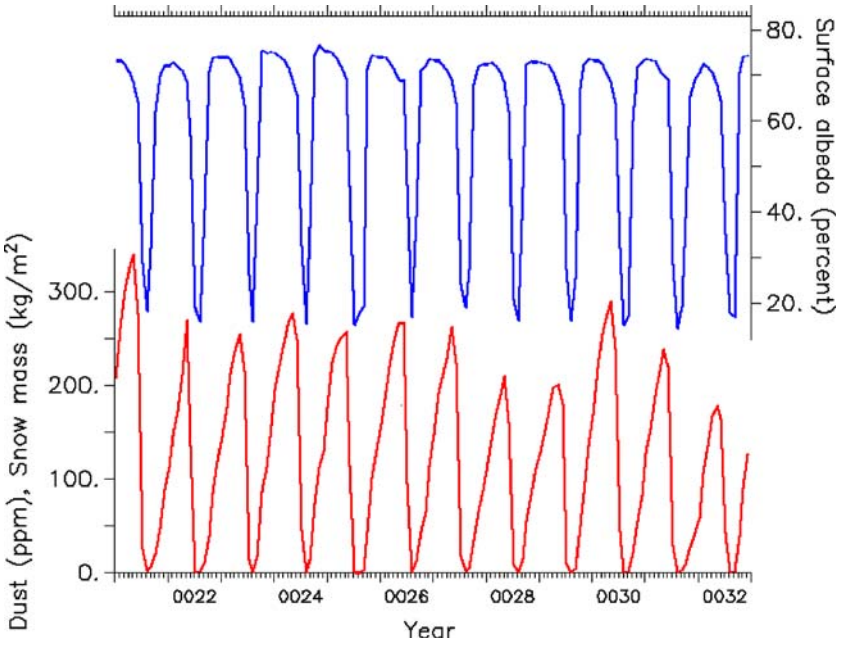

Fig. 7 Surface albedo, snow mass and dust content in surface snow. Monthly mean values of simulated broadband surface albedo (*blue*, %), dust content in surface snow (*black*, mg/kg), and snow mass (*red*, kg/m^2) in simulation D1.5/21k at 166°E and 63.5°N

As stated before, the first significant dust peak in the GRIP ice core from Central Greenland occurs at about this time (Fuhrer et al. 1999), and this corresponds to a period of fast retreat of the Barents-Kara Ice Sheet in Western Siberia (Mangerud et al. 2001; Svendsen et al. 2004). Our ''reduced deposition'' LGM simulation, which we have to use as a surrogate for a proper 90 kyr BP simulation, suggests dust-induced recession of permanent snow cover in the region from which the ice sheet retreated at about 90 kyr BP. We can therefore suggest that, in conjunction with an increase of summer insolation (Berger 1978), the higher dust deposition at that time might have caused the ice sheet to retreat. This is similar to the explanation for glacial termination after the LGM suggested by Peltier and Marshall (1995). Dust concentrations were generally high during the rest of the glacial period. The results presented here suggest that the north- and westward recession of the ice sheet during the course of the glacial period might be a consequence both of drying and increased dust deposition in later glacial stages, with dust deposition being particularly strong in the Southeast, closer to the Asian dust sources. Conversely, the initial growth of the ice sheet over the Barents and Kara Seas (i.e. relatively far to the East) during the Early Weichselian (i.e. before 90 kyr BP) appears to have been favoured by low dust deposition rates at that time.

Over Eastern Siberia, the model does not suggest systematic drying; regionally, simulated LGM precipitation even exceeds present-day values. Here, the model simulates snow-free peak summer conditions during the LGM only when dust deposition is taken into account. Dust deposition thus seems to play a decisive role in the climate dynamics in this region.

Because of the greater distance to dust source regions and the higher surface altitude, which constitutes an obstacle for dust transport, glacial dust deposition rates were lower on the ice sheets than over ice-free regions (Fig. 1). Thus, the impact of dust deposition on snow albedo and mass balance had a larger spatial extent in regions with seasonal snow cover, as shown here, than on ice sheets as discussed by Peltier and Marshall (1995) in the context of glacial termination. However, glacial dust deposition on the low-lying ice sheet margins, and its consequences in terms of snow and ice melt and subsequent ice margin retreat, might have been substantial.

Overpeck et al. (1996) suggested that heavy atmospheric dust loading during the last glacial period could have induced abrupt warming of a few °C over snow- and ice-covered regions. Claquin et al. (2003) showed that the net radiative forcing of LGM dust aerosol is negative on the global scale, with positive forcing occurring only over regions with high surface albedo (mainly bare soils or soil covered by snow or ice). If we crudely identify the regions of dust positive radiative forcing with the regions where warming occurs, our results indicate that, in the region of interest, the warming induced by atmospheric dust aerosols, not simulated here, would be accom-

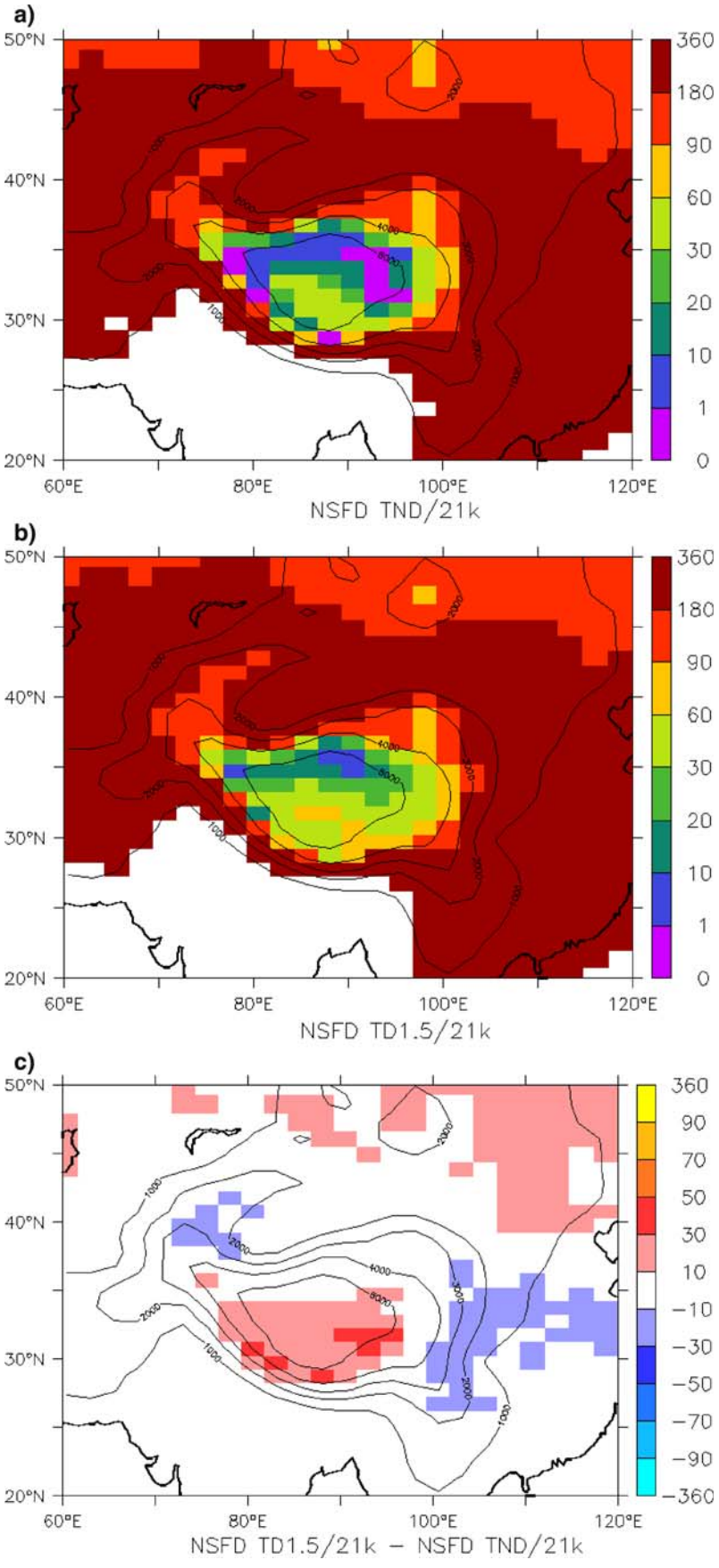

Fig. 8 *NSFD* over Tibet. As in Fig. 6, but for the simulations focused on Tibet. **a** *NSFD* simulated in TND/21k, **b** *NSFD* simulated in TD1.5/21k and **c** *NSFD* difference: TD1.5/21k – TND/21k. The *contour lines* represent surface altitude (every 1,000 m) and allow to situate Tibet easily on the map. *White zones* in (**a**) and (**b**) indicate oceanic grid points or continental grid points without any snow at all during the whole year

panied by an additional warming caused by snow albedo decrease due to dust deposition on snow. The radiative effect of dust aerosol probably had a weaker seasonality than the effect linked to dust deposition on snow, even though, as stated before, dust storms in Central Asia are most frequent in spring and early summer (Qian et al. 2002), at least today. Moreover, the effect of dust deposited on the snow surface is reinforced during snow melt (which is the critical period) because the dust tends to accumulate near the melting surface. There is no such positive feedback for the radiative impact of atmospheric aerosols during the critical season.

Hansen and Nazarenko (2004) and Jacobson (2004) have shown that soot deposition today plays a role in the observed winter warming in recent decades. Contrary to soot, which tends to be flushed trough the snow pack fairly rapidly (Jacobson 2004), small particles of mineral dust tend to stay near the surface (Aoki et al. 2003; Jacobson 2004), as stated before. This leads to a positive feedback during snow melt, with snow melt inducing higher surface dust concentrations, which in turn causes enhanced snow melt. Therefore, the climatic impact of dust deposition on snow is particularly strong during the melt season (and indirectly in summer in regions where this effect is causal for the disappearance of the seasonal snow pack), not in winter as is the case for soot.

Figure 6 tends to suggest that the probable absence of a major ice sheet on the Tibetan Plateau during the glacial period (Lehmkuhl and Owen 2005) is favoured by the high dust deposition rates. To analyse the impact of dust deposition on snow in Tibet in more detail, we carried out two additional 17-year-long simulations, one with 1.5% haematite content in dust and one without dust, with high regional resolution over the Tibetan Plateau instead of northern Asia (simulations TND/21k and TD1.5/21k). For northern Asia, these additional simulations essentially confirm the results of the simulations focused on that region. However, the area of permanent snow cover on the Tibetan Plateau is considerably smaller in TND/21k (Fig. 8) than in the corresponding simulation with high resolution over northern Asia (ND/21k, Fig. 6). Therefore, although the model does suggest a reduction of the duration of snow cover due to dust deposition on snow, this effect need not be invoked to understand why Tibet was ice-free at the LGM. We note however that even in TD0/21k, the model does suggest permanent snow on some grid points, in particular in eastern Tibet. It is possible that coupling with an ice sheet model would reveal that glacial inception occurs in this area, leading to ice cover over a larger area. Interestingly, control simulations with a regular resolution of about 300 km also suggested significant permanent snow cover over Tibet during the LGM when dust deposition on snow was not taken into account. The simulation focused on Tibet does not confirm these results. This highlights the importance of high resolution in regions with complex orography.

5 Concluding summary

Dust deposition on snow leads to particularly low surface albedo during the melt season in spring and summer. Our simulations suggest that periods of strong dust deposition in northern Asia prevented the establishment of permanent snow cover in this region. The model generally simulates more than 30 days without snow cover in summer at places subject to permanent snow cover when dust deposition, and its impact on snow albedo, is not taken into account. Although we carried out simulations only for the LGM (21 kyr BP), additional simulations with reduced dust deposition rates indicate that this effect operated during much of the last glacial period. This study thus presents evidence that the impact of dust deposition on snow albedo during glacial periods was crucial in determining the position of the last great ice sheets, and in particular, in determining the regions where ice sheets could not exist. The strong Asian dust sources may have prevented ice sheet formation over this continent.

During the early Weichselian (at about 85 kyr BP), dust-induced melt (in combination with increased summer insolation) possibly contributed to the demise of the Barents-Kara ice sheet during the course of the glacial period, while ice sheets developed and were sustained further away, over Fennoscandia, Greenland and North America. This effect might thus have contributed to the westward shift of the Eurasian ice sheets during the course of the Weichselian, with initial strong glaciation over the Barents and Kara Seas, and an ice sheet centered on Fennoscandia at the LGM (Svendsen et al. 2004).

Acknowledgments This project was supported by the Fonds National de la Science (ACI Changement Climatique et Cryosphère). The simulations were carried out on the MIRAGE computer platform in Grenoble. We thank N. Mahowald for making her simulated present and glacial dust deposition fields available to us. The authors acknowledge the help of B. Crouzille in coding the snow albedo routine.

References

Aoki T, Hachikubo A, Hori M (2003) Effects of snow physical parameters on shortwave broadband albedos. J Geophys Res 108:4616. DOI 10.1029/2003JD003506

Armstrong RL, Brodzik MJ (2002) Northern Hemisphere EASE-Grid weekly snow cover and sea ice extent version 2. National Snow and Ice Data Center. CD-ROM, Boulder, CO, USA

Beck C, Grieser J, Rudolf B (2005) A new monthly precipitation climatology for the global land areas for the period 1951 to 2000. German Weather Service, Offenbach, Germany. Digital media, http://www.dwd.de/en/FundE/Klima/KLIS/int/GPCC/GPCC.htm

Berger A (1978) Long-term variations of daily insolation and Quaternary climatic changes. J Atmos Sci 35:2362–2367

Brun E, Martin E, Simon V, Gendre C, Coleou C (1989) An energy and mass model of snow cover suitable for operational avalanche forecasting. J Glaciol 35:333–342

Calov R, Ganopolski A, Claussen M, Petoukhiv V, Greve R (2005) Transient simulation of the last glacial inception. Part I: glacial inception as a bifurcation in the climate system. Clim Dyn 24:545–561

Chalita S, Le Treut H (1994) The albedo of temperate and boreal forest in the northern hemisphere climate: a sensitivity experiment using the LMD AGCM. Clim Dyn 10:231–240

Claquin T, Schulz M, Balkanski Y (1999) Modeling the mineralogy of atmospheric dust sources. J Geophys Res 104:22243–22256

Claquin T, Roelandt C, Kohfeld KE, Harrison SP, Tegen I, Prentice IC, Balkanski Y, Bergametti G, Hansson M, Mahowald N, Rodhe H, Schulz M (2003) Radiative forcing of climate by ice-age atmospheric dust. Clim Dyn 20:193–202

Clark PU, Lix AC (2002) Ice sheets and sea level of the Last Glacial Maximum Quat. Sci. Rev 21:1–7

CLIMAP Project Members (1984) The last interglacial ocean. Quat Res 21:123–224

Crowley T (1995) Ice age terrestrial carbon changes revisited. Glob Biogeochem Cyc 9:377–389

Douville H, Royer J-F, Mahfouf J-F (1995) A new snow parameterization for the Météo-France climate model, Part 1: validation in stand-alone experiments. Clim Dyn 12:37–52

Fuhrer K, Wolff E, Johnsen SJ (1999) Timescales for dust variability in the Greenland Ice Core Project (GRIP) ice core in the last 100,000 years. J Geophys Res 104:31043–31052

Gates WL (1992) AMIP: the atmospheric model intercomparison project. Bull Am Met Soc 73:1962–1970

Guelle W, Balkanski Y, Schulz M, Marticorena B, Bergametti G, Moulin C, Arimoto R, Perry KD (2000) Modelling the atmospheric distribution of mineral aerosol: comparison with ground measurements and satellite observations for yearly and synoptic time scales over the North Atlantic. J Geophys Res 105:1997–2005

Hansen J, Nazarenko L (2004) Soot climate forcing via snow and ice albedos. Proc Nat Acad Sci 101:423–428

Harrison SP, Kohfeld KE, Roelandt C, Claquin T (2001) The role of dust in climate changes today, at the last glacial maximum and in the future. Earth Sci Rev 54:43–80

Harvey LDD (1988) Climatic impact of ice-age aerosols. Nature 334:333–335

Haywood J., Boucher O (2000) Estimates of the direct and indirect radiative forcing due to tropospheric aerosols: a review. Rev Geophys 38:513–543

Hourdin F, Musat I, Bony S, Braconnot P, Codron F, Dufresne JL, Fairhead L, Filiberti MA, Friedlingstein P, Grandpeix JY, Krinner G, Le Van P, Li ZX, Lott F (2006) The LMDZ4 general circulation model: climate performance and sensitivity to parametrized physics with emphasis on tropical convection. Clim Dyn

Hubberten HW, Andreev A, Astakhov VI, Demidov I, Dowdeswell JA, Henriksen M, Hjort C, Houmark-Nielsen M, Jakobsson M, Kuzmina S, Larsen E, Lunkka JP, Lysså A, Mangerud J, Möller P, Saarnisto M, Schirrmeister L, Sher AV, Siegert C, Siegert MJ, Svendsen JI (2004) The periglacial climate and environment in northern Eurasia during the Last Glaciation. Quat Sci Rev 23:1333–1357

Jacobson MZ (2004) Climate response of fossil fuel and biofuel soot, accounting for soot's feedback to snow and sea ice albedo and emissivity. J Geophys Res 109:D21201. DOI 10.1029/2004JD004945

Jacquinet-Husson N et al (1999) The 1997 spectroscopic GEISA databank. J Quant Spect Radiat Transfer 61:425–438

Joussaume S, Taylor KE (1995) Status of the paleoclimate modeling intercomparison project (PMIP). In: Gates WL (ed) Proceedings of the first international AMIP scientific conference, Monterey, CA, pp 425–430. PMIP database: http://www-lsce.cea.fr/pmip

Krinner G, Mangerud J, Jakobsson M, Crucifix M, Ritz C, Svendsen JI (2004) Enhanced ice sheet growth in Eurasia owing to adjacent ice dammed lakes. Nature 427:429–433

Liao H, Seinfeld JH (1998) Radiative forcing by mineral dust aerosols: sensitivity to key variables. J Geophys Res 103:31637–31646

Legates DR, Willmott CJ (1990) Mean seasonal and spatial variability in global surface air temperature. Theor Appl Climatol 41:11–21

Lehmkuhl F, Owen LA (2005) Late Quaternary glaciation of Tibet and the bordering mountains: a review. Boreas 34:87–100

Mahowald N, Kohfeld KE, Hansson M, Balkanski Y, Harrison SP, Prentice IC, Schulz M, Rodhe H (1999) Dust sources and deposition during the last glacial maximum and current climate: a comparison of model results with paleodata from ice cores and marine sediments. J. Geophys. Res. 104:15895–15916

Makeyev VM, Bolshiyanov DY (1986) Characteristics of glacial sediments on the Severnaya Zemlya Archipelago. In: Kainozoi shel'fa i ostronov Rossiiskoi Arktiki. Leningrad, pp 127–132

Mangerud J, Astakhov V, Murray A, Svendsen JI (2001) The chronology of a large ice-dammed lake and the Barents-Kara ice sheet advances. Glob Planet Change 31:321–336

Marshall S, Oglesby RJ (1994) An improved snow hydrology for GCMs. Part I: snow cover fraction, albedo, grain size, and age. Clim Dyn 10:21–37

Mayewski PA, Meeker LD, Whitlow S, Twickler MS, Morrison MC, Bloomfield P, Bond GC, Alley RB, Gow AJ, Grootes PM, Meese DA, Ram M, Taylor KC, Wumkes W (1994) Changes in atmospheric circulation and ocean ice cover over the North Atlantic during the last 41,000 years. Science 263:1747–1751

Overpeck JT, Rind D, Lacis A, Healy R (1996) Possible role of dust-induced regional warming in abrupt climate change during the last glacial period. Nature 384:447–449

Peltier WR (2004) Global glacial isostasy and the surface of the ice-age Earth: the ICE-5G (VM2) model and GRACE. Ann Rev Earth Planet Sci 32:111–149

Peltier WR, Marshall S (1995) Coupled energy-balance/ice-sheet model simulations of the glacial cycle: a possible connection between terminations and terrigenous dust. J Geophys Res 100:14269–14290

Petit JR, Jouzel J, Raynaud D, Barkov NI, Barnola JM, Basile I, Beznder M, Chappellaz J, Davis M, Delaygue G, Delmotte M, Kotlaykov VM, Legrand M, Lipenkov VY, Lorius C, Pépin L, Ritz C, Saltzman E, Stievenard M (1999) Climate and atmospheric history of the past 420,000 years from the Vostok ice core. Nature 399:426–436

Qian W, Quan L, Shi S (2002) Variations of the dust storm in China and its climatic control. J Climate 15:1216–1229

Roesch A, Wild M, Gilgen H, Ohmura A (2001) A new snow cover fraction parameterization for the ECHAM4 GCM. Clim Dyn 17:933–946

Siegert MJ, Marsiat I (2001) Numerical reconstructions of LGM climate across the Eurasian Arctic. Quat Sci Rev 20:1595–1605

Stauch G, Lehmkuhl F, Frechen M (2005) Pleistocene glacial advances in the Verkhoyansk Mountains, North-Eastern Siberia. Geophys Res Abstr 7:09061

Steffensen JP (1997) The size distribution of microparticles from selected segments of the Greenland Ice Core Project ice core representing different climatic periods. J Geophys Res 102:26755–26763

Svendsen JI, Alexanderson H, Astakhov VI, Demidov I, Dowdeswell JA, Funder S, Gataullin V, Henriksen M, Hjort C, Houmark-Nielsen M, Hubberten HW, Ingólfsson O, Jakobsson M, Kjær KH, Larsen E, Lokrantz H, Lunkka JP, Lyså A, Mangerud J, Matiouchkov A, Murray A, Möller P, Niessen F, Nikolskaya O, Polyak L, Saarnisto M, Siegert C, Siegert MJ, Spielhagen RF, Stein R (2004) Late Quaternary ice sheet history of Eurasia. Quat Sci Rev 23:1229–1271

Takemura T, Nozawa T, Emori S, Nakajima TY, Nakajima T (2005) Simulation of climate response to aerosol direct and indirect effects with aerosol transport-radiation model. J Geophys Res 110:D02202. DOI 10.1029/2004JD005029

Tarasov PE, Peyron O, Guiot J, Brewer S, Volkova VS, Bezusko LG, Dorofeyuk NI, Kvavadze EV, Osipova IM, Panova NK (1999) Last Glacial Maximum climate of the former Soviet Union and Mongolia reconstructed from pollen and plant macrofossil data. Clim Dyn 15:227–240

Warren WG, Wiscombe SG (1980) A model for the spectral albedo of snow. II: snow containing atmospheric aerosols. J Atmos Sci 37:2734–2745

Wiscombe SG, Warren WG (1980) A model for the spectral albedo of snow. I: pure snow. J Atmos Sci 37:2712–2733